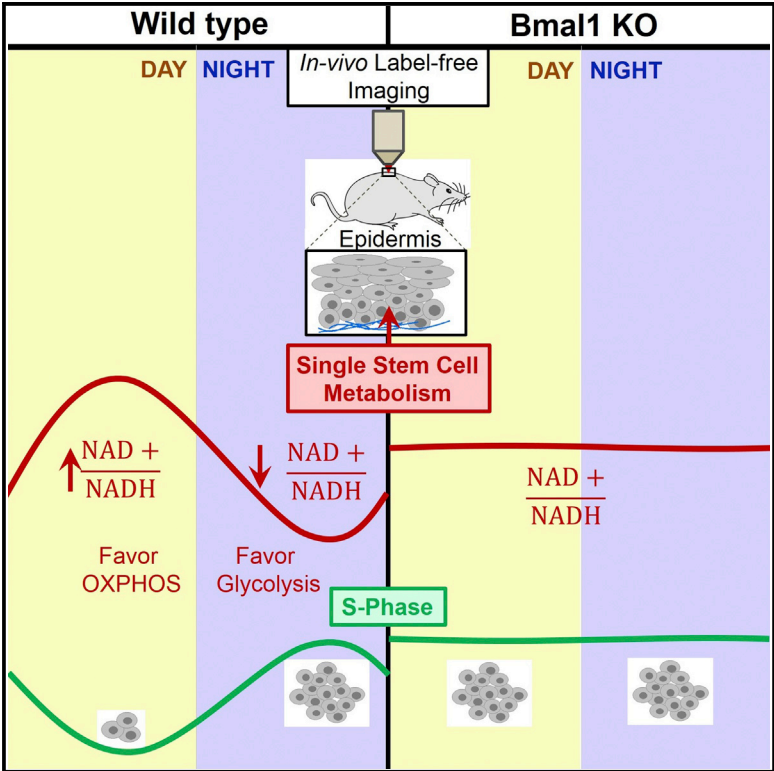# Cell Reports

In Vivo Single-Cell Detection of Metabolic Oscillations in Stem Cells

Graphical Abstract

Authors

Chiara Stringari, Hong Wang, ..., Bogi Andersen, Enrico Gratton

Correspondence

bogi@uci.edu (B.A.),
egratton@uci.edu (E.G.)

In Brief

The role of the circadian clock in stem cell metabolism is unclear. Stringari et al. use a label-free, noninvasive method to demonstrate circadian clock regulation of intermediary metabolism in epidermal stem cells in vivo. The clock coordinates intermediary metabolism and cell-cycle progression, perhaps to minimize genotoxicity.

Highlights

- We used a noninvasive method to study epidermal stem cell metabolism in vivo

- The circadian clock regulates intermediary metabolism in epidermal stem cells

- A high NADH/NAD+ ratio, reflecting increased glycolysis, is found during the night

- This high NADH/NAD+ ratio correlates with a higher proportion of stem cells in S phase

CrossMark

CellPress

In Vivo Single-Cell Detection of Metabolic Oscillations in Stem Cells

Chiara Stringari,[1,2] Hong Wang,[3,4] Mikhail Geyfman,[3] Viera Crosignani,[1] Vivek Kumar,[5,6] Joseph S. Takahashi,[5,6] Bogi Andersen,[3,7,8,9,10,*] and Enrico Gratton[1,8,10,*]

[1]Laboratory of Fluorescence Dynamics, Biomedical Engineering Department, University of California, Irvine, Irvine, CA 92037, USA
[2]Laboratory for Optics and Biosciences, École Polytechnique, 91128 Palaiseau Cedex, France
[3]Department of Biological Chemistry, School of Medicine, University of California, Irvine, Irvine, CA 92037, USA
[4]State Key Laboratory for Agrobiotechnology, College of Biological Sciences, China Agricultural University, Beijing 100193, China
[5]Department of Neuroscience, University of Texas Southwestern Medical Center, Dallas, TX 75390, USA
[6]Howard Hughes Medical Institute, University of Texas Southwestern Medical Center, Dallas, TX 75390, USA
[7]Department of Medicine, School of Medicine, University of California, Irvine, Irvine, CA 92037, USA
[8]Center for Complex Biological System, University of California, Irvine, Irvine, CA 92037, USA
[9]Institute for Genomics and Bioinformatics, University of California, Irvine, Irvine, CA 92037, USA
[10]Co-senior author
*Correspondence: bogi@uci.edu (B.A.), egratton@uci.edu (E.G.)
http://dx.doi.org/10.1016/j.celrep.2014.12.007

SUMMARY

Through the use of bulk measurements in metabolic organs, the circadian clock was shown to play roles in organismal energy homeostasis. However, the relationship between metabolic and circadian oscillations has not been studied in vivo at a single-cell level. Also, it is unknown whether the circadian clock controls metabolism in stem cells. We used a sensitive, noninvasive method to detect metabolic oscillations and circadian phase within epidermal stem cells in live mice at the single-cell level. We observe a higher NADH/NAD+ ratio, reflecting an increased glycolysis/oxidative phosphorylation ratio during the night compared to the day. Furthermore, we demonstrate that single-cell metabolic heterogeneity within the basal cell layer correlates with the circadian clock and that diurnal fluctuations in NADH/NAD+ ratio are *Bmal1* dependent. Our data show that, in proliferating stem cells, the circadian clock coordinates activities of oxidative phosphorylation and glycolysis with DNA synthesis, perhaps as a protective mechanism against genotoxicity.

INTRODUCTION

The circadian clock is a self-sustained cellular oscillator that coordinates appropriate metabolic responses within peripheral tissues with the light/dark cycle. Recent studies demonstrated that the circadian clock and metabolism are tightly interconnected (Bass and Takahashi, 2010; Eckel-Mahan and Sassone-Corsi, 2013; Sahar and Sassone-Corsi, 2009). Thus, circadian-clock-regulated transcription feedback loops in the liver produce cycles of NAD+ biosynthesis, ATP production, and mitochondrial respiration, and conversely, the cellular redox status influences the activity of clock transcription factors (Peek et al., 2013). So far, in vivo evaluations of metabolic oscillations have been done through bulk-tissue experiments. Furthermore, it remains unknown whether the circadian clock is involved in metabolism control in stem cells that maintain self-renewing epithelia.

The interfollicular epidermis, a prototype proliferative epithelium, contains a basal cell layer where the majority of cells are highly proliferative stem or progenitor cells that exit the cell cycle as they move into the suprabasal compartment for differentiation and formation of a protective barrier (Clayton et al., 2007; Lim et al., 2013; Mascre et al., 2012). Studies in a number of different mammals demonstrated a striking time-of-day-dependent variation in stem cell proliferation in the epidermis (Bjarnason and Jordan, 2002; Brown, 1991) and other proliferative epithelia such as the intestine (Potten et al., 1977). More recent studies have started to cast light on how the time-of-day-dependent variation in cell proliferation is regulated, showing that core circadian clock components are required for this feature (Gaddameedhi et al., 2011; Geyfman et al., 2012; Janich et al., 2011, 2013; Plikus et al., 2013).

The biological function of time-of-day-dependent stem cell proliferation remains unexplained (Gaddameedhi et al., 2011; Geyfman et al., 2012; Janich et al., 2013; Plikus et al., 2013). One hypothesis is that organisms have evolved to temporally separate DNA synthesis from metabolic functions such as oxidative phosphorylation as a protective mechanism, as has been suggested for metabolic cycles in yeast (Tu et al., 2005). Energy production through oxidative phosphorylation creates high levels of reactive oxygen species (ROS), which damage DNA, leading to cellular toxicity, cancer, and aging. A previous study reported that the expression of genes involved in oxidative phosphorylation and the skin's ROS levels are BMAL1 dependent and antiphasic to the peak in S phase for stem cells (Geyfman et al., 2012). The limitation of these studies is that, except for the quantitation of cell proliferation, they are based on measurements in
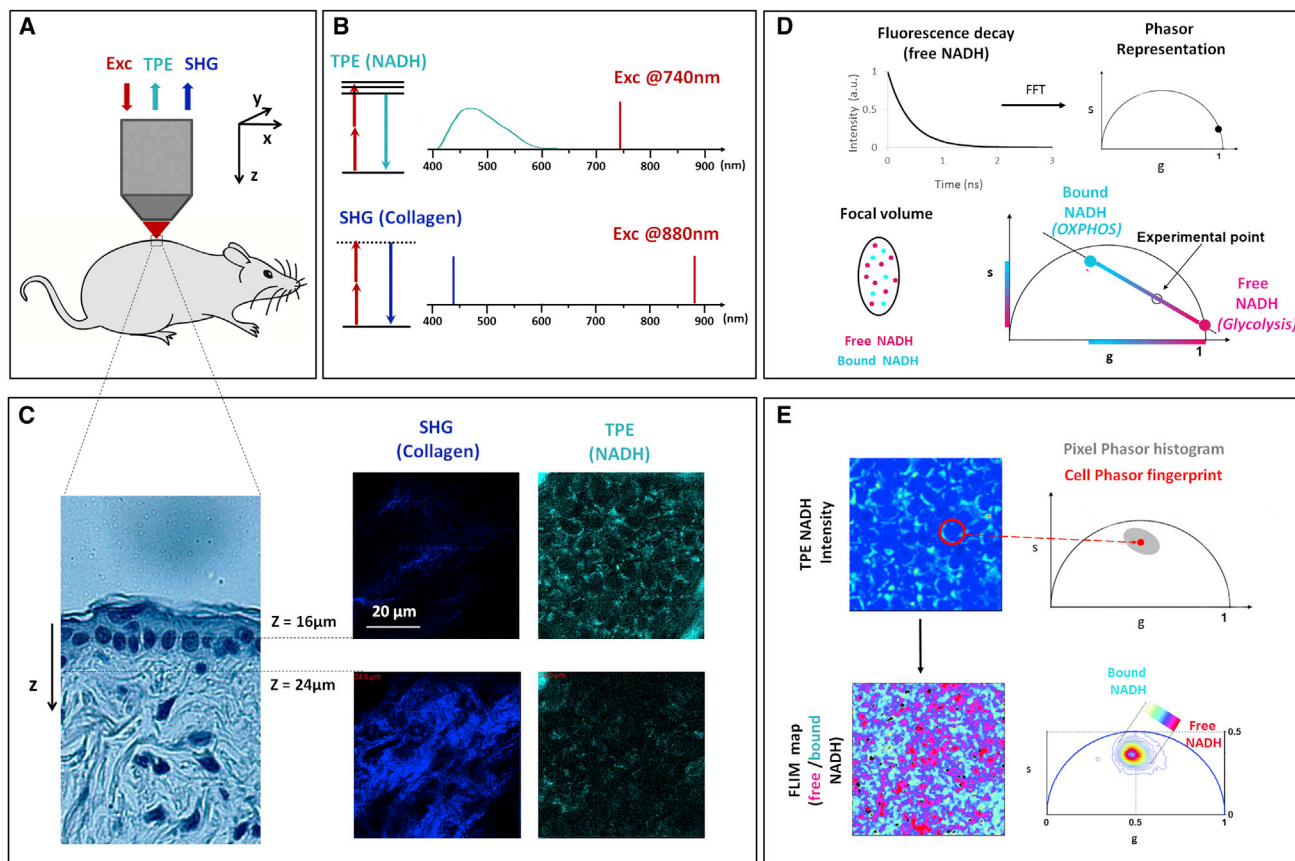
CrossMark

Figure 1. In Vivo Noninvasive NADH Imaging of Stem Cells within the Epidermal Basal Cell Layer

(A) Scheme of the live mouse imaging. Two-photon excitation (TPE) fluorescence from NADH (cyan) and second harmonic generation (SHG) from collagen are collected in epidetection through the same objective of the excitation (Exc), represented in red.

(B) Energy diagrams and wavelengths involved in the TPE and SHG.

(C) A representative cross-section of mouse skin showing the epidermis separated from the dermis by a basal lamina. SHG signal from dermal collagen fibers is excited at 880 nm and collected with a 440/20 nm filter. NADH TPE fluorescence intensity is excited at 740 nm and collected with a 460/80 nm filter highlighting single stem cells within the basal layer.

(D) After a mathematical transformation that involves fast Fourier transformation (FFT) (Experimental Procedures; Digman et al., 2008), the measured fluorescence lifetime decay is represented by a single point in the 2D phasor plot with g and s coordinates corresponding to the real and imaginary part of the FFT. Because of the linearity of the phasor coordinates, mixtures of free and bound NADH in the focal volume will lay along the line that connects the pure molecular species (Stringari et al., 2011).

(E) Phasor analysis of the FLIM images is performed both at the pixel level and cell level. Single pixels are painted in the FLIM map according to a linear cursor (from purple to cyan) that corresponds to different relative concentration of free and bound NADH. Optical metabolic fingerprint of single cells is calculated by averaging the phasor coordinates over the segmented region of interest of the cells (red circular cursor). Cell-phasor fingerprints are represented in the phasor scatterplot by single points located along the metabolic trajectory between glycolysis and oxidative phosphorylation (OXPHOS).

See also Figure S1.

the cellularly complex skin and rely on inference from gene expression rather than direct measurements of metabolites.

In order to study metabolism of stem cells of the epidermal basal cell layer in vivo, we applied two-photon excitation (TPE) and fluorescence lifetime imaging microscopy (FLIM) of the intrinsic metabolic biomarker NADH (Heikal, 2010; Konig and Riemann, 2003; Stringari et al., 2011; Figure 1). This optical method is noninvasive and provides sensitive and quantitative measurement of free and protein-bound NADH levels, which reflect the metabolic state of single cells within the native microenvironment of the living tissue (Stringari et al., 2011, 2012a). The free and bound NADH ratio reflects the NADH/NAD+ redox ratio

(Bird et al., 2005; Skala et al., 2007), an indicator of the relative level of glycolysis and oxidative phosphorylation within the cell (Bird et al., 2005; Stringari et al., 2012a; see Supplemental Information).

RESULTS

We first performed in vivo imaging of NADH autofluorescence and collagen second harmonic generation (SHG) in adult mouse skin (Figures 1A–1C) to determine whether we could utilize the SHG from the dermis to localize cells of the basal cell layer. This approach was successful, as NADH is excited at 740 nm within
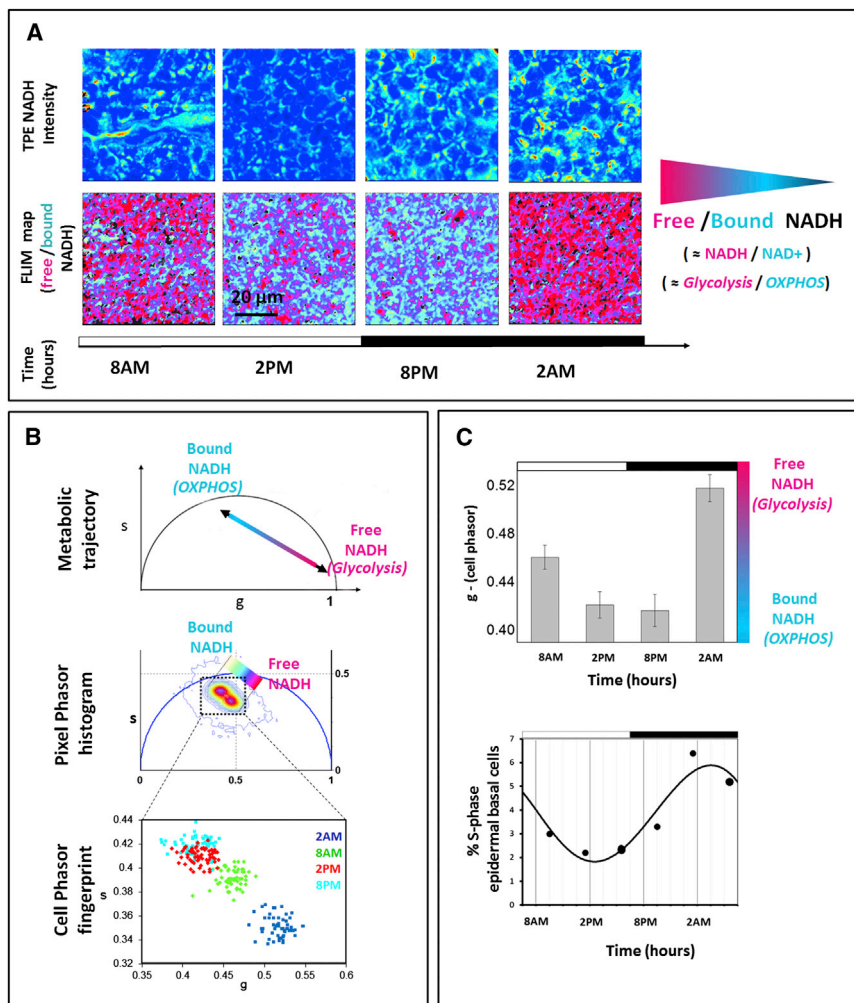
Figure 2. Free-to-Bound NADH Metabolic Circadian Oscillations in Stem Cells of the Epidermis Basal Layer

(A) TPE fluorescence intensity in vivo images of stem cells within the epidermis basal layer excited at 740 nm with respective FLIM color maps at 740 nm of the relative concentrations of free NADH and bound NADH. Red-purple color indicates a high free/bound NADH ratio, whereas violet, cyan, and white indicate linearly and progressively decreasing free/bound NADH ratios. Different ratios of free and protein-bound NADH reflect different redox ratios (NADH/NAD+) and rates of glycolysis and oxidative phosphorylation.

(B) Different relative concentrations of free and bound NADH correspond to a metabolic trajectory in the phasor plot between glycolysis and OX-PHOS, respectively. The linear cluster in the pixel phasor histogram represents all possible relative concentrations of free NADH (purple) and bound NADH (white). Scatterplot of the cell phasor of all stem cells optical metabolic fingerprint at different times of the day: 2 a.m. (blue); 8 a.m. (green); 2 p.m. (red); and 8 p.m. (cyan).

(C) The top shows a histogram of the g coordinate of the cell phasor fingerprint (which is proportional to the free/bound NADH ratio) displaying a circadian metabolic oscillation. All distributions are statistically different (t test p < 0.0001). The error bars indicate the SD. The bottom shows the average number of stem cells in S phase over 24 hr as determined by bromodeoxyuridine incorporation (Geyfman et al., 2012).

See also Figure S2.

cells of the epidermal basal cell layer, located right above the collagen fibers of the dermis (Figures 1C and S1). The two-photon fluorescence intensity NADH distribution highlights single-cell morphology with relatively dim nuclei and bright mitochondria (Figures 1C, 1E, and 2A). Analysis of the FLIM images is performed by a fast Fourier transform (FFT) of the FLIM raw data (Figures 1D and 1E) by creating a 2D histogram (phasor plot) of the NADH FLIM image where every pixel of the FLIM image is transformed into a pixel in the phasor plot (Figures 2A and 2B). The phasor coordinates g (x) and s (y) are the real and the imaginary part of the FFT transformation (Supplemental Information), respectively, and the g coordinate is the most sensitive to free/bound NADH variations (Stringari et al., 2011, 2012a). The broad NADH lifetime distribution (Figures 1D and 2B) has a characteristic linear-elongated pattern that reflects a mixture of free and bound NADH, yielding information on different distributions of metabolic states and redox ratios of the cells over the time (Stringari et al., 2012a).

We next used fluorescence lifetime measurement of intrinsic NADH within single cells (Figures 1D and 1E) of the basal cell layer to determine whether there are time-of-day-dependent fluctuations in NADH levels (Figure 2). We found that metabolic oscillations in the NADH cellular fingerprints follow a diurnal pattern, showing a consistent variation in free/bound NADH ratios between day and night (Figures 2 and S2). Mapping the relative concentration of free (purple) and bound (cyan) NADH within cells of the basal cell layer at different time points of the day, according to the FLIM phasor location of the free NADH and the bound NADH measured in solution (Stringari et al., 2011), we found greater free-to-bound NADH ratios at 2 a.m. and 8 a.m. than 2 p.m. and 8 p.m. (Figures 2A and 2B). In these studies, the metabolic optical fingerprint of single stem cells is measured through the average phasor FLIM value of the entire cell, including cytoplasmic, mitochondrial, and nuclear NADH (Figure 1E). Mitochondrial NADH is the major contributor to the cellular metabolic optical fingerprint because mitochondria are brighter than cytoplasm and nucleus and occupy a higher percentage of the cell volume (Figure 1C). For quantification, the cellular phasor values were then plotted in the scatter diagram, showing that the average FLIM phasor values of basal cells are significantly different according to the hours of the day, indicating a different metabolic state (t test between the g coordinate of single cells; p < 0.0001; Figure 2B). We found consistent results in six independent measurements (Figure S2). The relative concentration of free/bound NADH within stem cells is highest during the night at 2 a.m. and 8 a.m., decreasing significantly during the day at
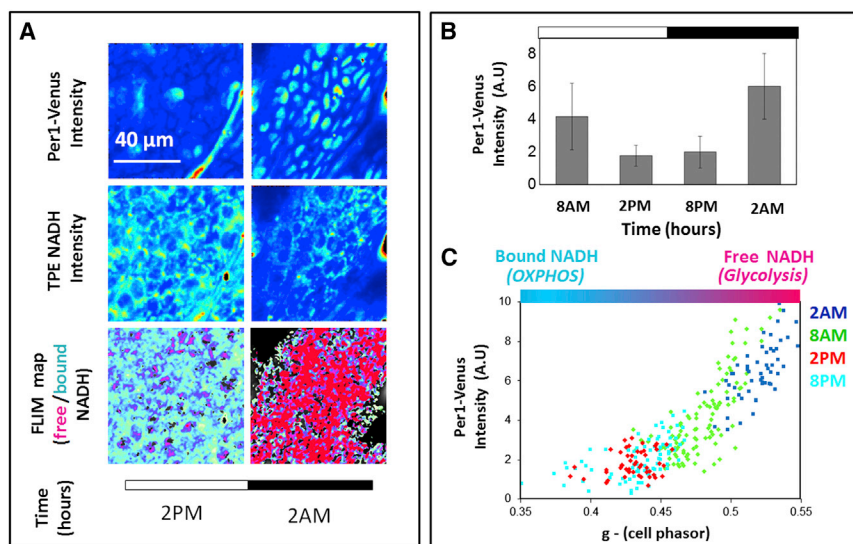
Figure 3. Metabolic Cell Heterogeneity in Epidermal Stem Cells Correlates with the Clock Phase

(A) TPE in vivo images of the epidermis basal cell layer expressing Per1-Venus reporter after excitation of stem cells at 940 nm. For the same field of view, TPE intensity images of NADH and FLIM color maps at 740 nm of the relative concentrations of free NADH and bound NADH are represented. Red-purple color indicates a high free/bound NADH ratio, whereas violet, cyan, and white indicate linearly and progressively decreasing free/bound NADH ratios.

(B) Histogram of the average Per1-Venus intensity from single stem cells displays a circadian oscillation in phase with the oscillation of the g coordinate of cell phasor fingerprint (Figure 2). The error bars indicate the SD. A.U, arbitrary units.

(C) Single-stem-cell Per1-Venus intensity displays a linear correlation with its metabolic fingerprint. See also Figure S3.
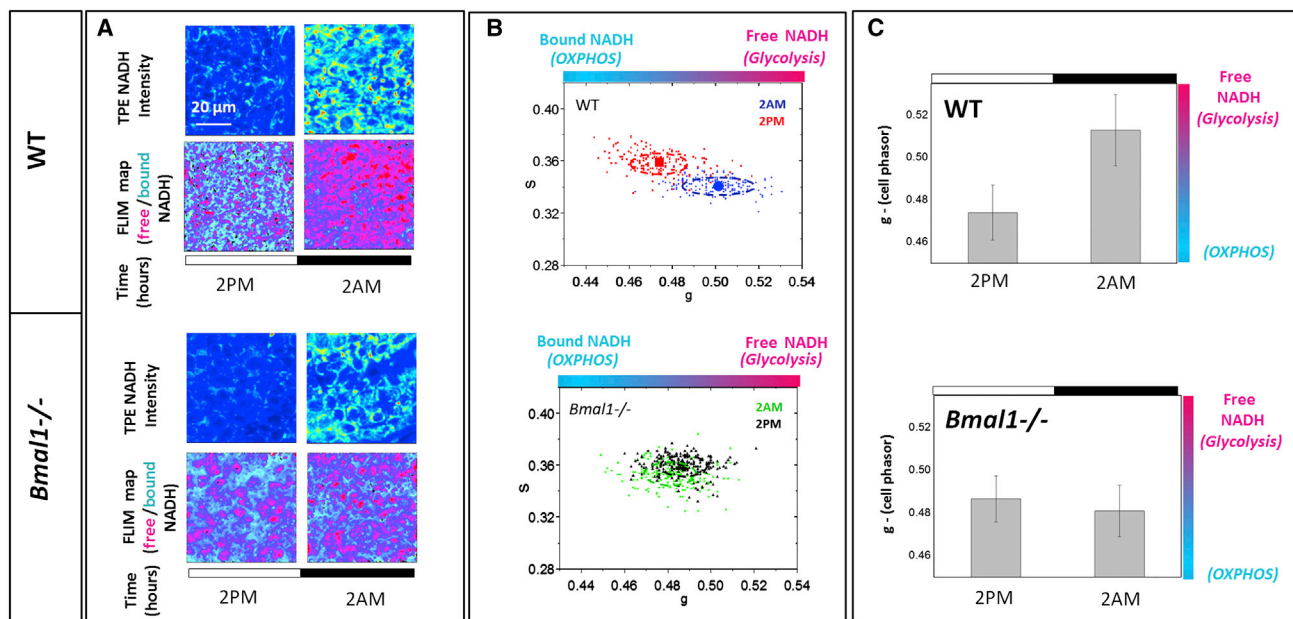
2 p.m. and 8 p.m. (Figures 2B and 2C). The histogram of the g coordinate of the cell phasor fingerprints (which is proportional to the free/bound NADH ratio) displays a circadian metabolic oscillation with a peak at 2 a.m. in phase with the highest percentage of cells in S phase (Figure 2C).

Different ratios of free and protein-bound NADH reflect different redox ratios (NADH/NAD+), which in turn reflect the relative rates of glycolysis and oxidative phosphorylation (glycolysis/oxidative phosphorylation [OXPHOS] ratio; Bird et al., 2005; Stringari et al., 2012a; see Supplemental Information). The time-of-day-dependent free/bound NADH oscillations suggest that cells of the basal cell layer have relatively higher rate of glycolysis during the night whereas during the day they present relatively higher rates of oxidative phosphorylation. The glycolytic and the oxidative phosphorylation phenotypes measured during the night and day (Figure 2), respectively, correlate with previously described time-of-day variation in S phase in epidermal stem cells with the high OXPHOS state being antiphasic to maximum S phase (Figure 2C; Geyfman et al., 2012). The metabolic oscillations that we measure in vivo in basal cell layer stem cells are also consistent with the NAD+ circadian rhythmicity and the mitochondrial oxidative respiration rates recently measured in liver cells (Peek et al., 2013).

The phasor FLIM analysis at single-cell resolution reveals significant cell-to-cell heterogeneity in the metabolic signature as indicated by the intrinsic free and protein-bound NADH concentrations (Figures 1D, 1E, and 2B). To quantify the intercell metabolic heterogeneity within the basal cell layer, we determined the SD of the phasor coordinates g over the entire population of recorded cells. The measured SD of the g cell phasor coordinates has a typical value between 0.008 and 0.034 (Figures 2B and S2), which is significantly larger than the experimental error on a single-cell phasor measurement (0.002 with the signal-to-noise ratio of the experiment; Stringari et al., 2012b). Hence, the free/bound NADH distribution we observe reflects a biological variation and true heterogeneity of the cellular metabolic fingerprint within the population of basal cells.

To investigate whether there is a correlation between the metabolic fingerprint and the circadian phase, we performed NADH FLIM measurements on the epidermis of Per1-Venus mice expressing the fluorescent protein VENUS from the clock-controlled Per1 promoter (Cheng et al., 2009). The circadian clock phase of individual progenitors of the basal cell layer was evaluated by exciting the tissue at 940 nm wavelength and measuring the intensity of the Per1-Venus reporter (see Experimental Procedures; Figure S3). As reported before (Cheng et al., 2009), the average intensity of the Per1-Venus reporter is higher at 2 a.m. and 8 a.m. than 2 p.m. and 8 p.m. (Figures 3A and 3B). The phase of the Per1-Venus clock reporter correlates with high ratios of free-to-bound NADH and glycolysis/OXPHOS ratios (i.e., high values of g coordinate of single-cell phasor fingerprints). Furthermore, we found a linear correlation between the cellular metabolic fingerprint (g coordinate of single-cell phasor) and the circadian-clock phase of individual cells (Per1-Venus reporter intensity; Figure 3C). Thus, the circadian clock output and the redox state show significant cell-to-cell heterogeneity and are tightly correlated at a cellular level.

To determine whether the daily fluctuations of NADH in progenitor cells of the basal cell layer are controlled by the circadian clock, we evaluated the metabolic fingerprint of epidermal stem cells in *Bmal1−/−* mice, which lack circadian rhythm (Bunger et al., 2000). We found that time-of-day-dependent metabolic oscillations of the progenitor cells in the epidermal basal cell layer are obliterated in the *Bmal1−/−* mice, (in Figure 4, the difference between the *Bmal1−/−* cell fingerprints at 2 a.m. and 2 p.m. is not statistically significant [t test p = 0.37]); these results were consistently observed in three independent measurements (Figure S4). As the *Bmal1−/−* mice were kept under normal 12:12 light-dark (LD) conditions, during which the animals are entrained as measured by wheel running, these experiments show that BMAL1 is required for diurnal variation in the free-to-bound ratio of NADH in stem cells of the interfollicular epidermis.

Figure 4. NADH Metabolic Oscillations Are Disrupted in the *Bmal1−/−* Epidermal Basal Layer

(A) Two-photon fluorescence intensity in vivo images of stem cells within the epidermis basal cell layer of wild-type (WT) and *Bmal1−/−* mice excited at 740 nm at two different time points. Phasor FLIM color maps at 740 nm of the relative concentrations of free NADH and bound NADH. Red-purple color indicates a high free/bound NADH ratio, whereas violet, cyan, and white indicate linearly and progressively decreasing free/bound NADH ratios.

(B) Scatterplot of the cell phasor of all stem cells' optical metabolic fingerprint at different times of the day: 2 a.m. (blue) and 2 p.m. (red) measured in WT mice (t test p < 0.0001) and 2 a.m. (green), 2 p.m. (black) measured in *Bmal1−/−* mice (t test p = 0.37).

(C) The circadian metabolic oscillation of the cell phasor fingerprint g coordinate (proportional to the free/bound NADH ratio) is disrupted in *Bmal1−/−* mice. The error bars indicate the SD.

See also Figure S4.

DISCUSSION

Previous studies have shown that proliferation of interfollicular epidermal stem cells is highly diurnal, with a greater percentage of cells undergoing S phase during the night than during the day in mice, and that this diurnal variation in cell proliferation depends on the core circadian clock gene *Bmal1* acting within keratinocytes (Gaddameedhi et al., 2011; Geyfman et al., 2012; Plikus et al., 2013). Whereas there is controversy about the hierarchy of cells within the basal layer of the interfollicular epidermis, previous work generally supports the idea that, during normal homeostasis, the mouse epidermis is primarily maintained by a single type of progenitor/stem cell (Clayton et al., 2007; Lim et al., 2013; Mascre et al., 2012). In this study, we have used FLIM, a label-free, single-cell resolution technique that detects the levels of bound and free NADH in vivo, to identify diurnal metabolic oscillations in stem cells of the interfollicular epidermis. The implementation of FLIM overcomes limitations of previous studies into the role of the circadian clock in metabolism based on bulk measurements, allowing the detection of metabolic heterogeneity within stem cells of the epidermis and correlation of this heterogeneity to clock output at a single-cell level.

Our study supports the idea that the circadian clock regulates metabolism within stem cells of the interfollicular epidermis for the following reasons. First, we find a correlation between the

NADH/NAD+ redox ratio as measured by FLIM and clock output as measured by activity of the Per1-Venus reporter in vivo. Second, we find that mutations in *Bmal1* disrupt the diurnal variation in the NADH/NAD+ redox ratio. Through regulation of gene expression within metabolic organs, the circadian clock has been shown to play a key role in diurnal shifts in organismal metabolic patterns (Peek et al., 2013; Sahar and Sassone-Corsi, 2009). Our study indicates that the circadian clock also has a key function in the modulation of metabolism within stem cells of a highly proliferative epithelial tissue. We show significant cell-to-cell heterogeneity in circadian output and NADH/NAD+ redox ratios, perhaps reflecting different levels of stemness among the epidermal basal cells.

Interestingly, we find that the epidermal stem cells show a more glycolytic phenotype during night, when the highest numbers of cells are in S phase (Geyfman et al., 2012). It has long been observed that proliferating cells rely more on glycolysis than oxidative phosphorylation, such as in the Warburg effect in cancer cells (Warburg, 1956). ROS are a normal mitochondrial byproduct of oxidative phosphorylation during cellular respiration (Murphy, 2009). Whereas also serving normal signaling roles (D'Autreaux and Toledano, 2007), ROS is toxic to the cell, oxidizing a variety of macromolecules including DNA where it causes mutations. Thus, the accumulation of ROS-mediated cellular damage is thought to play a role in carcinogenesis and aging. All tissues are susceptible to ROS-induced

DNA damage, but because the S phase of the cell cycle is the most-susceptible cellular stage, highly proliferative tissues are likely most sensitive to ROS-induced mutagenesis, thus providing one possible explanation for proliferating cells' reliance on glycolysis (Hamanaka and Chandel, 2011). Our findings suggest that the circadian clock confers time-of-day-dependent shifts in glycolysis versus oxidative phosphorylation within proliferating epithelial stem cells, thus minimizing DNA damage during S phase. Conversely, in Bmal1 mutant mice, which show no temporal separation of glycolytic and oxidative metabolism, this protection is presumably lost, leading to increased DNA damage. Indeed, mutations in *Bmal1* have been associated with premature aging and increased DNA damage (Janich et al., 2011; Kondratov et al., 2006).

EXPERIMENTAL PROCEDURES

Animal Models and Procedures

Mice were kept under 12 hr:12 hr LD cycle (light on at 6:30 a.m.) with unrestricted access to food and water. Immediately before imaging, mice were anesthetized with ketamine. Hair was shaved and removed with Nair hair remover (Church & Dwight) on the back in a 2 cm^2 area, which was washed under warm water and dried with Kimwipes. Procedures were approved by the Institutional Animal Care and Use Committee (protocols 2002-2357-3 and 2001-2239). *Bmal1−/−* and Per1-Venus mice were previously described (Bunger et al., 2000; Cheng et al., 2009). *Bmal1−/−* mice and controls were studied during first telogen at ages 20–22 days.

Imaging

Imaging was performed with a Zeiss 710 microscope coupled to a Ti:sapphire laser system (Spectra-Physics Mai Tai). A 40 × 0.8 numerical aperture water immersion objective (LUMPlanFl Olympus) with 2 mm working distance was used. The excitation wavelengths were 880 nm and 740 nm with average power of about 5 mW. Fluorescence intensity images of NADH were acquired by exciting the tissue at 740 nm and placing a 460/80 nm emission filter in front of the detector. Second harmonic generation from collagen was excited at 880 nm and collected with an emission filter 440/20 nm or excited at 940 nm and collected with a band-pass filter 470/20 nm.

The stem cells within the epidermal basal cell layer are identified by their unique location immediately above the collagen-rich layer of the dermis; a second harmonic generation 3D stack was systematically acquired to localize the edge of the dermis layer in the Z axis (Figure S1). For example, in Figure S1C, the edge of the dermis is identified at a depth of 18 μm, corresponding to the last Z section of the dermis that contains collagen. To localize the epidermal basal layer, we moved the focus in Z between 2 and 4 μm above the edge of the dermis layer. (In Figure S1B, the epidermal basal layer is located between 14 and 16 μm.) The epidermal basal layer is characterized (Figure S1B) by small and round-shaped stem cells, whereas cells that undergo differentiation in the upper layers are larger. Six regions of interest of the epidermal basal layer were imaged within the 2 cm^2 skin. We imaged four mice for every time point and condition.

Fluorescence lifetime images were acquired with an ISS A320 FastFLIM system (Colyer et al., 2008). For image acquisition, the following settings are used: image size of 256 × 256 pixels and scan speed of 25 μs/pixel. A dichroic filter (690 nm) was used to separate the fluorescence signal from the laser light and the fluorescence. For the acquisition of FLIM images, fluorescence is detected by a photomultiplier (H7422P-40 of Hamamatsu), and a 610 nm short-pass filter is placed in front of the detector. A 495 nm long-pass filter separates the blue and the green fluorescence. NADH fluorescence was collected through a 460/80 nm filter. FLIM data are acquired and processed by the SimFCS software developed at the Laboratory of Fluorescence Dynamics. FLIM calibration of the system is performed by measuring the known lifetime of the fluorescein with a single exponential of 4.04 ns. FLIM data are collected until 100 counts in the brightest pixel of the image are acquired. Typically, the acquisition time

was of the order of few seconds. To quantify Per1-Venus intensity, we excited the epidermal basal layer with a wavelength of 940 nm, acquiring ten frames for each field of view (Figure S3C). The same laser power of 5 mW was used for all fields of view. We verified that the Venus fluorescence signal of cells was not affected by photobleaching or photodamage by scanning 20 frames on the same field of view (Figure S3C).

FLIM Phasor Data Analysis

Every pixel of the FLIM image is transformed in one pixel in the 2D histogram of the phasor plot through a mathematical transformation of the fluorescence intensity decay that involves FFT (Digman et al., 2008; Stringari et al., 2011; Supplemental Information). The coordinates g and s (x and y coordinates, respectively) in the phasor plot are the real and imaginary part of the FFT. The analysis of the phasor distribution is performed by cluster identification of free and bound NADH. Because of the linearity of the phasor coordinates, mixtures of free and bound NADH in the focal volume will distribute along the line that connects the pure molecular species. Fractional intensities of chemical species in every pixel of the image were evaluated with a graphical analysis in the phasor plot as described previously (Digman et al., 2008; Stringari et al., 2011). We performed image segmentation on the FLIM data by selecting the region of interest of cells within the tissue, using a cursor with circular shape. We then calculated the phasor average value within the entire cell, including NADH in mitochondria and nuclei. When measuring the cell phasor, all pixels of the cell (about 1,000) are taken in account and the signal-to-noise ratio of the FLIM signature of cells is higher than in single pixels. The average value of the SD of the NADH average cell phasor is calculated over the five different independent experiments in Figures 2 and S2.

SUPPLEMENTAL INFORMATION

Supplemental Information includes Supplemental Experimental Procedures and four figures and can be found with this article online at http://dx.doi.org/10.1016/j.celrep.2014.12.007.

AUTHOR CONTRIBUTIONS

C.S., M.G., V.K., J.S.T., B.A., and E.G. conceived of and designed the experiments and analyzed the data. C.S., H.W., M.G., and V.C. performed the experiments. C.S., B.A., and E.G. wrote the manuscript with input from all other authors.

REFERENCES

Bass, J., and Takahashi, J.S. (2010). Circadian integration of metabolism and energetics. Science *330*, 1349–1354.

Bird, D.K., Yan, L., Vrotsos, K.M., Eliceiri, K.W., Vaughan, E.M., Keely, P.J., White, J.G., and Ramanujam, N. (2005). Metabolic mapping of MCF10A human breast cells via multiphoton fluorescence lifetime imaging of the coenzyme NADH. Cancer Res. *65*, 8766–8773.

Bjarnason, G.A., and Jordan, R. (2002). Rhythms in human gastrointestinal mucosa and skin. Chronobiol. Int. *19*, 129–140.

Brown, W.R. (1991). A review and mathematical analysis of circadian rhythms in cell proliferation in mouse, rat, and human epidermis. J. Invest. Dermatol. *97*, 273–280.

Bunger, M.K., Wilsbacher, L.D., Moran, S.M., Clendenin, C., Radcliffe, L.A., Hogenesch, J.B., Simon, M.C., Takahashi, J.S., and Bradfield, C.A. (2000).

Mop3 is an essential component of the master circadian pacemaker in mammals. Cell *103*, 1009–1017.

Cheng, H., Alvarez-Saavedra, M., Dziema, H., Choi, Y.S., Li, A., and Obrietan, K. (2009). Segregation of expression of mPeriod gene homologs in neurons and glia: possible divergent roles of mPeriod1 and mPeriod2 in the brain. Hum. Mol. Genet. *18*, 3110–3124.

Clayton, E., Doupe, D.P., Klein, A.M., Winton, D.J., Simons, B.D., and Jones, P.H. (2007). A single type of progenitor cell maintains normal epidermis. Nature *446*, 185–189.

Colyer, R., Lee, C., and Gratton, E. (2008). A novel fluorescence lifetime imaging system that optimizes photon efficiency. Microsc. Res. Tech. *71*, 201–213.

D'Autreaux, B., and Toledano, M.B. (2007). ROS as signalling molecules: mechanisms that generate specificity in ROS homeostasis. Nat. Rev. Mol. Cell Biol. *8*, 813–824.

Digman, M., Caiolfa, V.R., Zamai, M., and Gratton, E. (2008). The phasor approach to fluorescence lifetime imaging analysis. Biophys. J. *94*, L14–L16.

Eckel-Mahan, K., and Sassone-Corsi, P. (2013). Metabolism and the circadian clock converge. Physiol. Rev. *93*, 107–135.

Gaddameedhi, S., Selby, C.P., Kaufmann, W.K., Smart, R.C., and Sancar, A. (2011). Control of skin cancer by the circadian rhythm. Proc. Natl. Acad. Sci. USA *108*, 18790–18795.

Geyfman, M., Kumar, V., Liu, Q., Ruiz, R., Gordon, W., Espitia, F., Cam, E., Millar, S.E., Smyth, P., Ihler, A., et al. (2012). Brain and muscle Arnt-like protein-1 (BMAL1) controls circadian cell proliferation and susceptibility to UVB-induced DNA damage in the epidermis. Proc. Natl. Acad. Sci. USA *109*, 11758–11763.

Hamanaka, R., and Chandel, N.S. (2011). Cell biology. Warburg effect and redox balance. Science *334*, 1219–1220.

Heikal, A.A. (2010). Intracellular coenzymes as natural biomarkers for metabolic activities and mitochondrial anomalies. Biomarkers Med. *4*, 241–263.

Janich, P., Pascual, G., Merlos-Suarez, A., Batlle, E., Ripperger, J., Albrecht, U., Cheng, H.Y., Obrietan, K., Di Croce, L., and Benitah, S.A. (2011). The circadian molecular clock creates epidermal stem cell heterogeneity. Nature *480*, 209–214.

Janich, P., Toufighi, K., Solanas, G., Luis, N.M., Minkwitz, S., Serrano, L., Lehner, B., and Benitah, S.A. (2013). Human epidermal stem cell function is regulated by circadian oscillations. Cell Stem Cell *13*, 745–753.

Kondratov, R.V., Kondratova, A.A., Gorbacheva, V.Y., Vykhovanets, O.V., and Antoch, M.P. (2006). Early aging and age-related pathologies in mice deficient in BMAL1, the core componentof the circadian clock. Genes Dev. *20*, 1868–1873.

Konig, K., and Riemann, I. (2003). High-resolution multiphoton tomography of human skin with subcellular spatial resolution and picosecond time resolution. J. Biomed. Opt. *8*, 432–439.

Lim, X., Tan, S.H., Koh, W.L., Chau, R.M., Yan, K.S., Kuo, C.J., van Amerongen, R., Klein, A.M., and Nusse, R. (2013). Interfollicular epidermal stem cells self-renew via autocrine Wnt signaling. Science *342*, 1226–1230.

Mascre, G., Dekoninck, S., Drogat, B., Youssef, K.K., Brohee, S., Sotiropoulou, P.A., Simons, B.D., and Blanpain, C. (2012). Distinct contribution of stem and progenitor cells to epidermal maintenance. Nature *489*, 257–262.

Murphy, M.P. (2009). How mitochondria produce reactive oxygen species. Biochem. J. *417*, 1–13.

Peek, C., Affinati, A.H., Ramsey, K.M., Kuo, H.Y., Yu, W., Sena, L.A., Ilkayeva, O., Marcheva, B., Kobayashi, Y., Omura, C., et al. (2013). Circadian clock NAD+ cycle drives mitochondrial oxidative metabolism in mice. Science *342*, 1243417.

Plikus, M., Vollmers, C., de la Cruz, D., Chaix, A., Ramos, R., Panda, S., and Chuong, C.M. (2013). Local circadian clock gates cell cycle progression of transient amplifying cells during regenerative hair cycling. Proc. Natl. Acad. Sci. USA *110*, E2106–E2115.

Potten, C.S., Al-Barwari, S.E., Hume, W.J., and Searle, J. (1977). Circadian rhythms of presumptive stem cells in three different epithelia of the mouse. Cell Tissue Kinet. *10*, 557–568.

Sahar, S., and Sassone-Corsi, P. (2009). Metabolism and cancer: the circadian clock connection. Nat. Rev. Cancer *9*, 886–896.

Skala, M.C., Riching, K.M., Gendron-Fitzpatrick, A., Eickhoff, J., Eliceiri, K.W., White, J.G., and Ramanujam, N. (2007). In vivo multiphoton microscopy of NADH and FAD redox states, fluorescence lifetimes, and cellular morphology in precancerous epithelia. Proc. Natl. Acad. Sci. USA *104*, 19494–19499.

Stringari, C., Cinquin, A., Cinquin, O., Digman, M.A., Donovan, P.J., and Gratton, E. (2011). Phasor approach to fluorescence lifetime microscopy distinguishes different metabolic states of germ cells in a live tissue. Proc. Natl. Acad. Sci. USA *108*, 13582–13587.

Stringari, C., Edwards, R.A., Pate, K.T., Waterman, M.L., Donovan, P.J., and Gratton, E. (2012a). Metabolic trajectory of cellular differentiation in small intestine by Phasor Fluorescence Lifetime Microscopy of NADH. Sci. Rep. *2*, 568.

Stringari, C., Nourse, J.L., Flanagan, L., and Gratton, E. (2012b). Phasor Fluorescence Lifetime Microscopy of free and protein-bound NADH reveals neural Stem Cell Differentiation Potential. PLoS ONE *7*, e48014.

Tu, B., Kudlicki, A., Rowicka, M., and McKnight, S.L. (2005). Logic of the yeast metabolic cycle: temporal compartmentalization of cellular processes. Science *310*, 1152–1158.

Warburg, O. (1956). On the origin of cancer cells. Science *123*, 309–314.